FULL PAPER

Open Access

Two current systems in the preliminary phase of sudden commencements in the magnetosphere

Shigeru Fujita[1,2]* ⓘ and Takashi Tanaka[3]

Abstract

The preliminary impulse of the sudden commencement is simply explained by the generation of the compressional wave due to sudden compression of the dayside magnetopause and mode conversion from the compressional wave to the Alfvén wave in the magnetosphere. However, this simple model cannot explain a time delay of the peak displacement and longer duration time in the higher latitudes in the pre-noon and post-noon sectors of the polar region. Based on the global magnetohydrodynamic simulation of the magnetosphere–ionosphere system reveals that this peculiar behavior of the geomagnetic variation of the preliminary impulse is associated with temporal deformation of the ionospheric field-aligned current distribution of the preliminary impulse into a crescent shape; its lower-latitude edge extends toward the anti-sunward direction, and its higher-latitude edge almost stays on the same longitude near noon. Numerical simulations revealed that the deformation of the field-aligned current distribution is derived from different behaviors of the two current systems of the preliminary impulse. The first current system consists of the field-aligned current connected to the field-aligned current of the preliminary impulse in the lower latitude side of the ionosphere, the cross-magnetopause current, and the magnetosheath current (type L current system). The cross-magnetopause current is the inertia current generated in the acceleration front of the solar wind due to the sudden compression of the magnetosheath. Thus, the longitudinal speed of the type L current system in the ionosphere is the solar wind speed in the magnetosheath projected into the ionosphere. In contrast, the current system of the preliminary impulse connected to the field-aligned current of the preliminary impulse at higher latitude (type H current system) consists of the upward/downward field-aligned current in the pre-noon/post-noon sector, respectively, and dawn-to-dusk field-perpendicular current along the dayside magnetopause. The dawn-to-dusk field-perpendicular current moves to the higher latitudes in the outer magnetosphere over time. The field-aligned current of the type H current system is converted from the field-perpendicular current due to convergence of the return field-perpendicular current heading toward the sunward direction in the outer magnetosphere; the return field-perpendicular current is the inertia current driven by the magnetospheric plasma flow associated with compression of the magnetopause behind the front region of the accelerated solar wind. The acceleration front spreads concentrically from the subsolar point. Consequently, as the return field-perpendicular current is converted to the field-aligned current of the type H current system, it does not move much in the longitudinal direction over time because the dawn-to-dusk field-perpendicular current of the type H current system moves to the higher latitudes. Therefore, the high-latitude edge of the current distribution of the preliminary impulse in the ionosphere moves only slightly. Finally, we clarified that the conversion between field-perpendicular current and field-aligned current of the type L current

*Correspondence: sfujita@ism.ac.jp
[1] Joint Support-Center for Data Science Research, Research Organization of Information and Systems (ROIS), Tachikawa, Tokyo 190-8518, Japan
Full list of author information is available at the end of the article

system mainly occurs in the region where the Alfvén speed starts to increase toward the Earth. A region with a steep gradient of the Alfvén speed like the plasmapause is not always necessary for conversion from the field-perpendicular current to the field-aligned current. We also suggest the possible field-aligned structure of the standing Alfvén wave that may occur in the preliminary impulse phase.

Keywords: Sudden commencement, Preliminary impulse, Magnetospheric current system, Longitudinal propagation speed, Computer simulation, Generation of the field-aligned current

Graphical Abstract

Two current systems in the preliminary phase of the Sudden Commencement
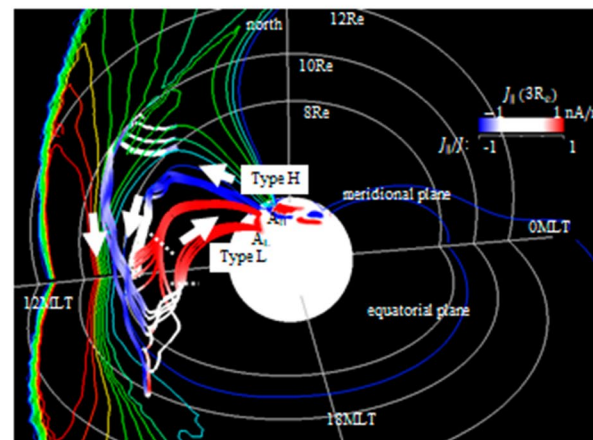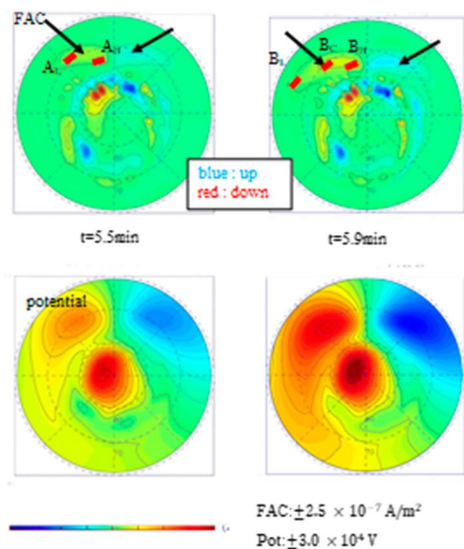
Longer duration and delay of peak time of PI geomagnetic variations in the higher latitudes are attributed to the latitudinal different propagation speed of the ionospheric FAC. Simulation reveals two different current systems bring about the peculiar behavior of the PI geomagnetic variations.

Introduction

The sudden commencement (SC) is an impulse response of the magnetosphere–ionosphere system caused by a sudden change of dynamic pressure of the solar wind (Chapman and Ferraro 1940). Therefore, the SC attracts the interest of many scientists as a unique tool for diagnosing the magnetosphere–ionosphere system [(Araki 1994), and references therein]. The characteristic ground magnetic signature of the SC is a simple stepwise change of the north–south component in the middle- and low-latitude regions [referred to as DL after Araki (1994)]. In contrast, the ground magnetic variation of the north–south component exhibits a bipolar change in the high-latitude region [DP after Araki (1994)]. The first and second variations of the bipolar DP change are called the preliminary impulse (PI) and the main impulse (MI).

In general, the PI is regarded to be accompanied by upward/downward field-aligned currents (FACs) in the pre-noon/post-noon ionosphere, respectively (Araki

1994). Tamao (1964) theoretically explained the cause of the PI current system. That is to say, the fast magnetosonic wave generated by sudden compression of the dayside magnetosphere is converted to the Alfvén wave with the upward/downward FAC propagating to the pre-noon/post-noon ionosphere, respectively.

Global magnetohydrodynamic (MHD) simulations have become a powerful tool for studying the SC (e.g., Fujita et al., 2003a,b). Fujita et al. (2003a) demonstrated that computer simulation can reproduce realistic ground magnetic variations in the SC period [hereafter Fujita et al. (2003a) is shortened as "Paper 1"]. Furthermore, they discussed that the essential mechanisms in the PI current system are fast magnetosonic waves generated by the sudden compression of the dayside magnetosphere, as well as mode conversion from the fast magnetosonic wave to the Alfvén wave due to the spatial gradient of the Alfvén speed, guided by the theory presented by Tamao (1964, 1965) and Araki (1994). Conversely, in the MI

phase, the localized convection vortex cell (the SC transient vortex) in the MI phase plays an essential role in the transient process of the magnetosphere–ionosphere system approaching the new stationary state after compression of the dayside magnetosphere by the solar wind with increased dynamic pressure (Fujita et al. 2003b).

Paper 1 found a PI current system that schematically resembles the current model by Araki (1994), but they did not further pursue the implications of the simulation results. For example, the longitudinal propagation speed of the PI current system in the magnetosphere will be as fast as that of the fast magnetosonic wave because the FAC is converted from the FPC of the fast magnetosonic wave in the front of the propagating fast magnetosonic wave. However, Engebretson et al. (1999) demonstrated that the longitudinal speed of the PI signal in the ionosphere corresponds to the solar wind speed, not that of the fast magnetosonic wave. In addition, there are issues that Paper 1 did not answer; Sastri et al. (2001) indicated that the duration of the ground magnetic variations of the PI in the afternoon (∼15 MLT) is longer at higher latitudes. Also, the peak of the variation is delayed at a higher latitude. Takeuchi et al. (2000) also presented the same behavior of the PI geomagnetic variations for the negative sudden impulse (SI). Recently, Belakhovsky et al. (2017) also demonstrated a delay in the geomagnetic peak variation of the PI toward the polar region for events in the morning sector (∼8.5 MLT). These features, that is, slow longitudinal propagation and peculiar latitudinal change of the PI signal, also seem to appear in the simulation results. For example, the latitudinal change of the PI variation presented in Fig. 2 of Paper 1 exhibits the peculiar behavior consistent with the observed one, although they did not mention this behavior. These features are not resolved yet by theoretical and simulation studies. Therefore, we are pursuing explanations of these features in the present paper.

Furthermore, Paper 1 discussed only qualitatively the conversion from FPC to FAC based on the mode conversion between the fast magnetosonic wave and the Alfvén wave in the non-uniform distribution of the Alfvén speed in the magnetosphere. Paper 1 concluded that the mode conversion mainly occurs in the region of the steep gradient at Alfvén speeds, and one candidate of the conversion region is the plasmapause. However, they did not study the conversion quantitatively. Because we have the simulation results that satisfy the physical principles of the conversion region, we can investigate quantitatively the conversion from FPC to FAC. This issue is also treated in this paper.

The present paper is structured as follows. "Preliminary impulse reproduced by the REPPU code" section demonstrates that the ground magnetic variations reproduced by the newly developed global MHD simulation named REProduce Plasma Universe (REPPU) (Tanaka 2015) can simulate the ground magnetic variation of the SC correctly. "Two current systems in the PI phase" section presents the PI current system in the magnetosphere to reveal the peculiar behaviors of the ground magnetic variations. "Discussion" section analyses in detail the FPC–FAC conversion in the PI current system. Propagation of the PI signal in the longitudinal direction is also summarized here. The last section summarizes the main results.

Preliminary impulse reproduced by the REPPU code

The present simulation study uses the global MHD simulation code REPPU newly developed by Tanaka (2015). This code solves the MHD equations with the ionospheric boundary condition in the magnetosphere–ionosphere system. The outer boundaries of the magnetosphere are located at 600Re in the dayside and 200Re in the nightside. The inner boundary is set on the sphere with a radius of 3Re. The simulated FAC on the lower boundary is transmitted along the field lines to the ionosphere. The electric field induced in the ionosphere by the FAC is again transmitted to the magnetosphere. The level 6 version of the REPPU code that we employed for this study has 61,440 triangular surface cells on one sphere and 240 radial layers, so the total number of grid elements is 14,745,600. (The horizontal mesh size is about 0.1Re on the sphere of $r = 10$Re, and the distance between the spheres is about 0.2Re.) Details of the REPPU code are explained in Tanaka (2015). We imposed a sudden increase in the solar wind plasma density from 10.0 to 25.0 cm^{-3} at $x = 25$Re from the Earth to drive the SC in the northern interplanetary magnetic field (IMF) condition (IMFBz = +4.3 nT). The other parameters used for the simulation are as follows: IMFBx = 0, IMFBy = − 4.3 nT, Vx = 372 km/s, Vy = Vz = 0 km/s, and the temperature of the solar wind is 10,000,000 K.

It is instructive to show the ground magnetic variations of the SC obtained by the present simulation by REPPU. Paper 1 also calculated the ground magnetic variations from the ionospheric Hall current. Strictly speaking, this method can be used under the condition of a uniform ionosphere and vertical incidence of the FAC into the ionosphere. These two assumptions do not hold in the simulation. To present more correct ground magnetic variations, we calculated the variations from the ionospheric Hall and Pedersen currents, as well as the FAC, based on the Biot–Savart law after Tanaka et al. (2020). [Tanaka et al. (2020) demonstrated that the ground magnetic variation of the SC is mainly produced by the ionospheric Hall current. Therefore, the present results in Fig. 1 and the result by Paper 1 are essentially similar.
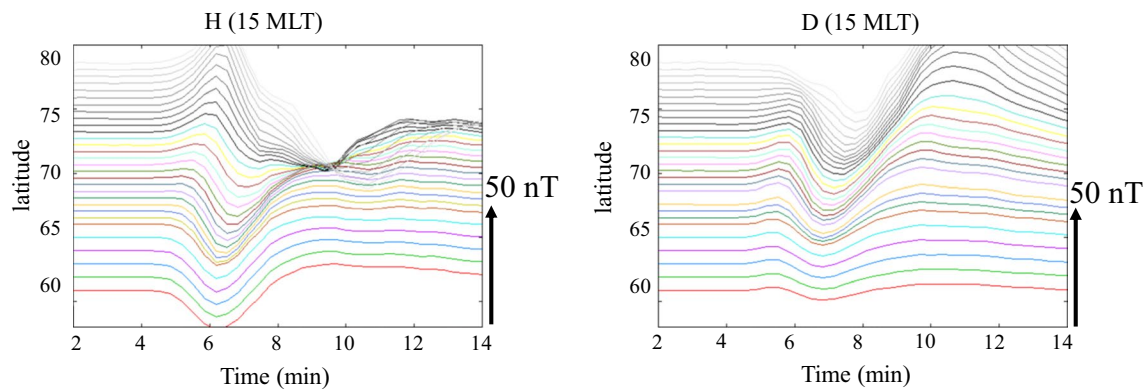
Fig. 1 Latitudinal dependences of the temporal variations of the H- and D-component ground magnetic fields associated with the SC in the latitudes from 60.8° to 78.5° in the northern hemisphere at 15 MLT. The vertical arrow in the right axis in each panel indicates the magnetic variation of 50 nT. The start time ($t=0$) is the time when the solar wind shock passes $x=25$Re
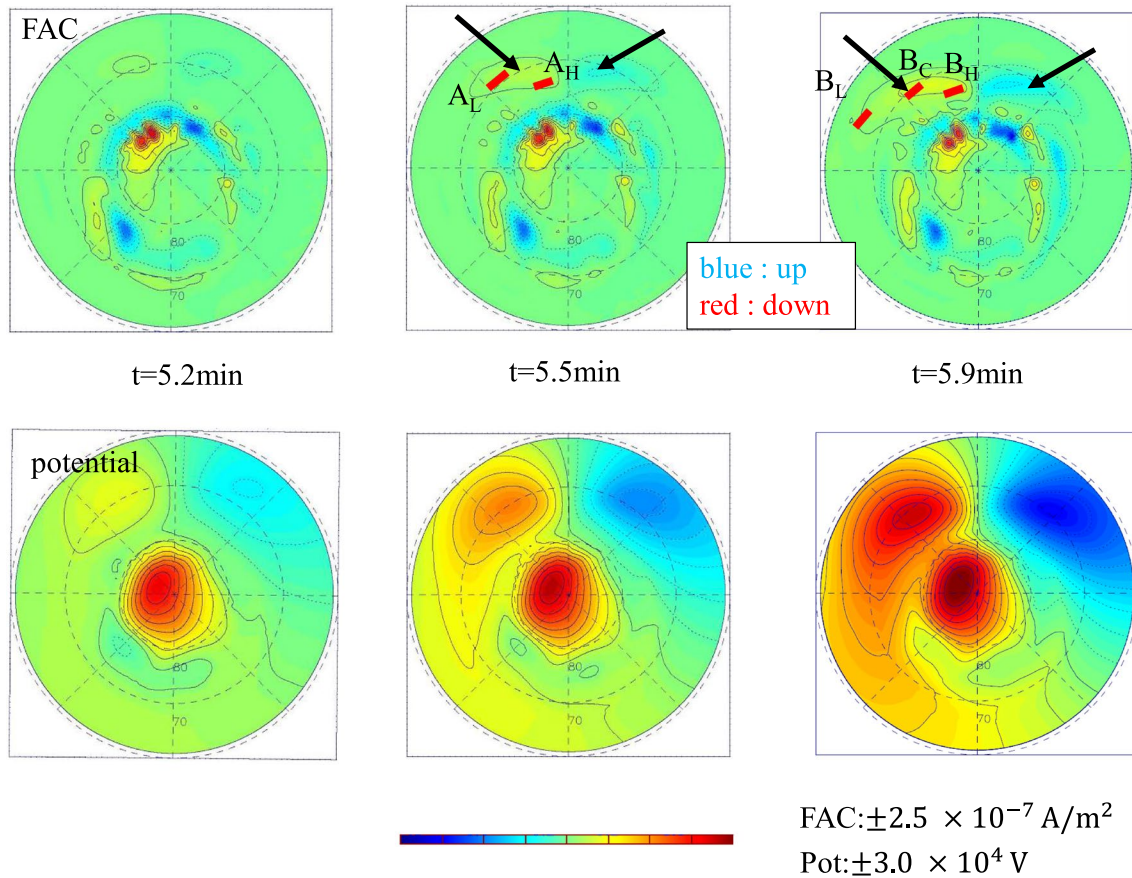

Fig. 2 (Top row) Temporal evolution of the FAC distribution in the northern hemisphere at latitudes above 60° from $t=5.2$ to 5.9 min. The black arrows at $t=5.5$ and 5.9 min indicate the FACs of the PI. The red thick lines labeled A_H and A_L in the 5.5-min panel and B_H, B_c, and B_L in the 5.9-min panel indicate the footpoints of the current systems shown in Figs. 3 and 4. The latitude and MLT of these footpoints are as follows: $A_H=$(75.5°, 12.6–13.1 MLT); $A_L=$(69.1°, 14.0–14.8 MLT); $B_H=$(73.6°, 12.6–13.1 MLT); $B_C=$(71.3°, 13.8–15.0 MLT); $B_L=$(65.9°, 16.2–16.8 MLT). (Bottom row) Temporal evolution of the electric potential distribution for the same region and time intervals

Note that the present results are more correct than those given in Paper 1]. Let us show the latitudinal dependence of temporal variations of the geomagnetic horizontal components at 15 MLT in the latitude range from 60.8° to 78.5° in Fig. 1 based on the simulation results by REPPU. The geomagnetic contribution from the magnetospheric current is not included in Fig. 1 because it essentially produces the DL geomagnetic variation. The start time ($t = 0$) is the time when the solar wind shock passes $x = 25$Re. Finally, let us discuss the calculated geomagnetic H variation of this figure. The H component variation at 15 MLT clearly shows the negative PI variation and the following MI variation in the latitudes below about 70° and similar to the typical variations at about 15 MLT presented by Araki (1994). Furthermore, we recognize that the duration of the PI geomagnetic variation at 15 MLT becomes longer at higher latitudes and the peak of the H variation becomes delayed (see the variations in the latitudes below 75°). Therefore, we can obtain the answers to the unresolved issues about the peculiar behaviors of the PI ground signal by analyzing the present simulation results.
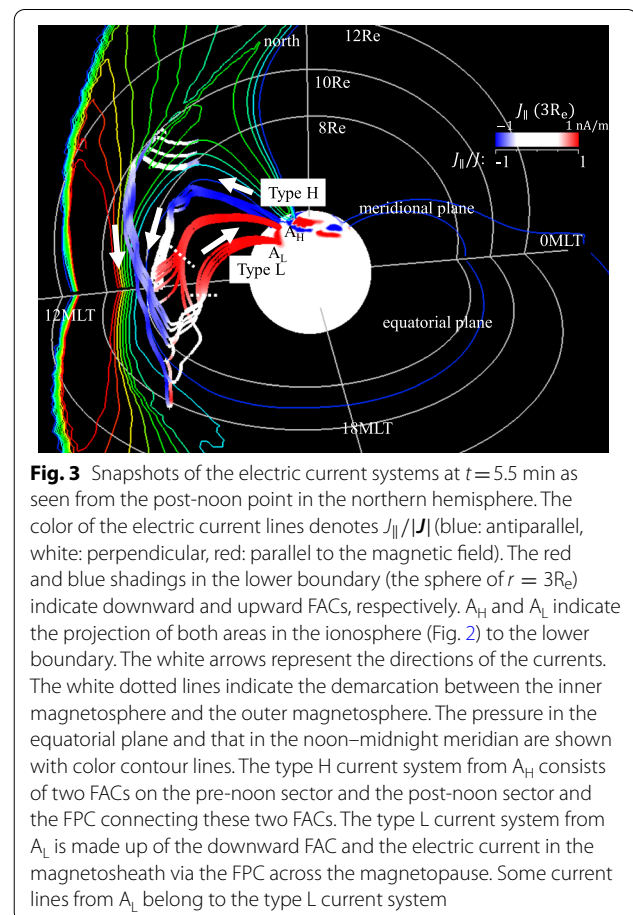
As noted above, the ground magnetic variation is mainly induced by the ionospheric Hall current. Therefore, we need to investigate the temporal variation of the ionospheric potential distribution. Next, as the potential is controlled by the FAC from the magnetosphere, the temporal variation of the FAC distribution is a key parameter for understanding the behavior of the ground magnetic variations as shown in Fig. 1. Following this guideline, we investigate the temporal variation of the FAC distribution and the electric potential distribution. Figure 2 shows these distributions in the northern ionosphere of the latitudes of 60°–90°. The FAC distribution and the potential distribution before the SC are depicted in the left panels at $t = 5.2$ min. Next, the typical PI current in the ionosphere (downward/upward FAC in the post-noon/pre-noon sector, respectively) appears at $t = 5.5$ and 5.9 min, as indicated by black arrows. We notice that the ionospheric PI current distribution depicts a crescent shape with the lower-latitude edge extending in the anti-sunward direction and the higher-latitude edge almost staying at the same longitude. Corresponding to this crescent shape of the ionospheric PI current, the potential distribution shows a similar shape: the positive/negative potential in the post-noon/pre-noon sector extends in the anti-sunward direction in the lower latitude side. Therefore, this varying ionospheric PI current will invoke the peculiar behavior of the PI geomagnetic variation. That is to say, because the FAC in the lower latitudes advances in the anti-sunward direction faster than the FAC at higher latitudes, the peak time of the PI magnetic disturbance appears earlier than
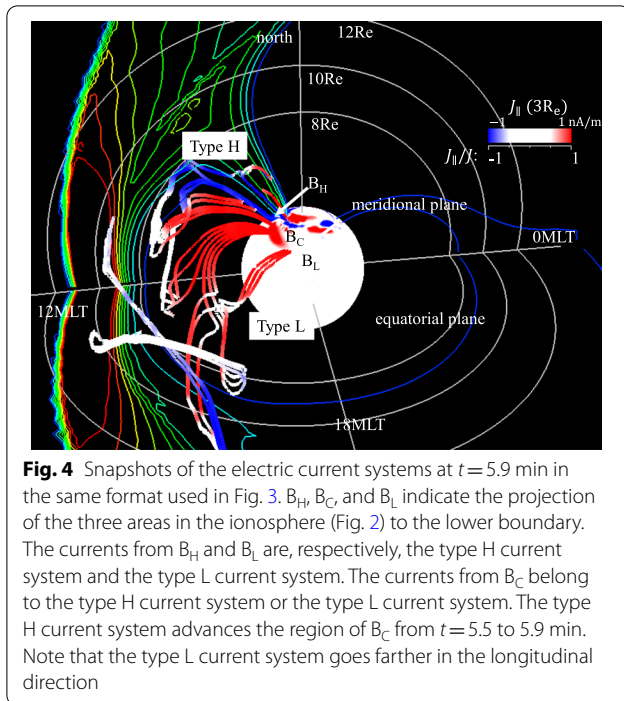
that at higher latitudes. Consequently, to understand the mechanism of the peculiar features of the PI geomagnetic variations, we need to clarify the mechanism in the magnetosphere that causes the latitudinal change of the PI current system.

Two current systems in the PI phase
Current systems obtained from the simulation results
Here, we investigate the magnetospheric current systems driving the ionospheric FAC distribution shown in Fig. 2 to clarify the mechanism of the temporal deformation of the crescent-shaped FAC distribution that yields the peculiar behavior of the ground magnetic variations in the PI phase. Because the longitudinal shift of the FAC distribution depends on the latitude, we investigated the magnetosphere–ionosphere current systems from the ionospheric footpoints located at the higher-latitude ionosphere (A_H) and the lower-latitude ionosphere (A_L) at $t = 5.5$ min and B_H (higher latitude), B_C (central latitude), and B_L (lower latitude) at $t = 5.9$ min, as marked in Fig. 2. The magnetospheric 3D current systems from these footpoints at $t = 5.5$ and 5.9 min are shown in Figs. 3 and 4,

Fig. 3 Snapshots of the electric current systems at $t = 5.5$ min as seen from the post-noon point in the northern hemisphere. The color of the electric current lines denotes $J_\parallel / |\mathbf{J}|$ (blue: antiparallel, white: perpendicular, red: parallel to the magnetic field). The red and blue shadings in the lower boundary (the sphere of $r = 3R_e$) indicate downward and upward FACs, respectively. A_H and A_L indicate the projection of both areas in the ionosphere (Fig. 2) to the lower boundary. The white arrows represent the directions of the currents. The white dotted lines indicate the demarcation between the inner magnetosphere and the outer magnetosphere. The pressure in the equatorial plane and that in the noon–midnight meridian are shown with color contour lines. The type H current system from A_H consists of two FACs on the pre-noon sector and the post-noon sector and the FPC connecting these two FACs. The type L current system from A_L is made up of the downward FAC and the electric current in the magnetosheath via the FPC across the magnetopause. Some current lines from A_L belong to the type L current system

Fig. 4 Snapshots of the electric current systems at $t=5.9$ min in the same format used in Fig. 3. B_H, B_C, and B_L indicate the projection of the three areas in the ionosphere (Fig. 2) to the lower boundary. The currents from B_H and B_L are, respectively, the type H current system and the type L current system. The currents from B_C belong to the type H current system or the type L current system. The type H current system advances the region of B_C from $t=5.5$ to 5.9 min. Note that the type L current system goes farther in the longitudinal direction

respectively. Note that the respective footpoints shown in Figs. 3 and 4 are the projections from the respective points in the ionosphere to the lower boundary of the simulation ($r=3$Re) along magnetic field lines. The color of current lines is denoted as $J_{\parallel}/|\boldsymbol{J}|$ (blue: antiparallel, white: perpendicular, red: parallel to the magnetic field), where $J_{\parallel}$ and $\boldsymbol{J}$ are the FAC and the current vector, respectively. For convenience, we call the region where a bundle of the current lines is along the main field lines the inner magnetosphere and the other region the outer magnetosphere. For example, the white broken lines in Fig. 3 indicate demarcations between the inner magnetosphere and the outer magnetosphere.
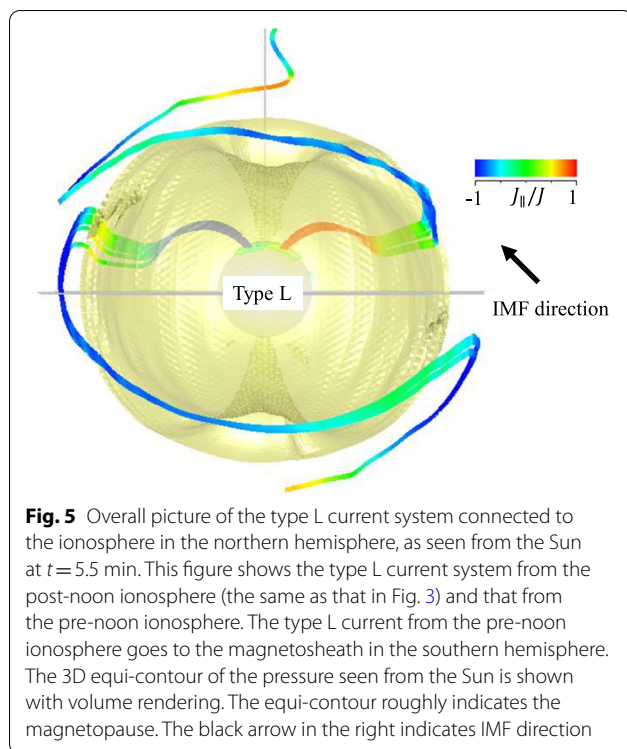
First, let us consider the current systems from A_H and A_L at $t=5.5$ min shown in Fig. 3. The current lines from A_H consist of the following three currents; the downward FAC (red) on the post-noon sector in the inner magnetosphere, the upward FAC (blue) on the pre-noon sector in the inner magnetosphere, and the FPC (white), that flow in the dawn-to-dusk direction in the outer magnetosphere. This current system with the footpoints in the higher-latitude ionosphere (A_H) is named the type H current system. The FPC seems to be converted to the FAC gradually in the outer magnetosphere. (The conversion occurs in the region of $L\approx8$.) The other current lines from the footpoint in the lower-latitude ionosphere (A_L) consist of the downward FAC in the post-noon sector of the inner magnetosphere, the FPC across the magnetopause, and the magnetosheath current. This current

system is called the type L current system. The cross-magnetopause current enters the magnetosphere and the FPC–FAC conversion occurs at the boundary between the inner and outer magnetospheres apart from the magnetopause. (The conversion occurs in the region of $L\approx7$.) The magnetosheath current tends to flow along the field lines. This tendency attributes to the generation of the FAC due to the flow shear of the solar wind in front of the magnetopause. (The magnetosheath current is discussed again below.) This current system is newly found by the present study. We noticed that the current lines from the anti-sunward edge of A_H go to the magnetosheath (the L current system). This result indicates that A_H is located at the boundary between the regime of the type H current system and that of the type L current system.

Next, Fig. 4 depicts the three current systems from B_H, B_C, and B_L at $t=5.9$ min. The current lines from B_H belong to the type H current system, and those from B_L are the type L current system. We note that the dawn-to-dusk FPC of the type H current system from B_H at $t=5.9$ min moves to a latitude higher than that from A_H at $t=5.5$ min. The cross-magnetopause current and the magnetosheath current of the type L current system seem disturbed compared with that at $t=5.5$ min. Probably, the solar wind in the magnetosheath begins to become irregular at $t=5.9$ min. It is noted that the current lines from B_C consist of both the type H current system and the type L current system. This result indicates that the regime of the type H current system advances toward the anti-sunward direction from A_H at $t=5.5$ min to B_C at $t=5.9$ min. Therefore, because B_C is located on the sunward side of B_L, the type H current system always appears behind the type L current system heading in the anti-sunward direction.

To summarize the results of Figs. 3 and 4, we can see that the current systems from A_H ($t=5.5$ min) and B_H ($t=5.9$ min) belong to the type H current system, whereas those from A_L ($t=5.5$ min) and B_L ($t=5.9$ min) belong to the type L current system. Consequently, because A_H and B_H are located in the same longitude, the immovable higher-latitude edge of the crescent-shaped distribution of the PI current system comes from the behavior of the type H current system. At the same time, the extension of the lower-latitude edge is derived from the behavior of the type L current system. Consequently, the PI current distribution becomes a crescent form with the stable higher-latitude edge and the lower-latitude edge moving in the anti-sunward direction due to the coexistence of the two current systems in a different manner of longitudinal spread.

Because Fig. 3 shows only the type L current system with the ionospheric footpoints on the post-noon sector, we show the conjugate type L current systems with the

Fig. 5 Overall picture of the type L current system connected to the ionosphere in the northern hemisphere, as seen from the Sun at $t = 5.5$ min. This figure shows the type L current system from the post-noon ionosphere (the same as that in Fig. 3) and that from the pre-noon ionosphere. The type L current from the pre-noon ionosphere goes to the magnetosheath in the southern hemisphere. The 3D equi-contour of the pressure seen from the Sun is shown with volume rendering. The equi-contour roughly indicates the magnetopause. The black arrow in the right indicates IMF direction

ionospheric footpoints on the pre-noon sector in Fig. 5 as well as that from the post-noon sector shown in Fig. 3. The 3D equi-contour surface of the pressure roughly corresponds to the dayside magnetopause. The current system in the post-noon sector goes to the magnetosheath in the northern hemisphere, whereas that in the pre-noon sector goes to the magnetosheath in the southern hemisphere. Both currents from both hemispheres flow along the field line in the magnetosheath. Because IMFBy is negative and IMFBz is positive in this simulation as shown in this figure, the current from the post-noon magnetosphere goes to the northern hemisphere. In other words, when IMFBy is positive (and IMFBz is positive), the current system in the post-noon/pre-noon sector goes to the southern/northern magnetosheath, respectively. The magnetosheath current finally connects to the solar wind.

Note that the current system treated here is a line connecting current vectors at an instant in time; in other words, we are examining snapshots of a constantly changing current line. Thus, although the current line of the type L current system crosses the magnetopause, this does not mean that plasmas in the magnetosheath enter the magnetosphere. When some accelerated plasmas in the magnetosheath deform the magnetopause, adjacent plasmas just inside and outside of the magnetopause move in the same direction. Deformation of the magnetic field associated with this movement will yield the

local electric current perpendicular to the magnetopause. However, the plasmas in the magnetosheath do not enter the magnetosphere.

Excitation processes of the two current systems

Now, we discuss how the sudden compression of the dayside magnetosphere excites the type H current system and the type L current system. The important issues are (1) why the type L current system crosses the magnetopause and (2) why the type H current system appears behind the type L current system and the ionospheric footpoint in the higher latitude does not move in the longitudinal direction. In this section, we mainly analyze the current systems at $t = 5.5$ min (Fig. 3) because disturbances in the magnetosphere caused by the sudden compression show typical and clear behavior at this time. To tackle these issues, we investigated the spatial patterns of the FPC vectors and the plasma flow vectors in the outer magnetosphere and the magnetosheath. We also analyzed the plasma disturbances in the equatorial plane, although the cross-magnetopause current of the type L current system and the FPC–FAC conversion of the type H current system does occur in the off-equatorial region. This is because both phenomena exist near the equatorial plane and the flow patterns and the FPC patterns in and around the equatorial plane are very similar.

In the beginning, let us examine the behavior of the FPC in the outer magnetosphere and the magnetosheath at $t = 5.5$ min. Figure 6 shows the FPC vectors

Fig. 6 FPC vectors in the post-noon sector of the equatorial plane at 5.5 min. $\nabla_\perp \cdot \boldsymbol{J}_\perp$ values in the equatorial plane are shown with color shading. The red circle indicates the equatorial projection of the region where the cross-magnetopause current exists. The type L current flows across the magnetopause in this region. In contrast, the blue ellipse indicates the equatorial projection of the region where the type H current system converts from the FPC to the FAC. It is evident that the current exhibits negative divergence ($\nabla \cdot \boldsymbol{J}_\perp < 0$) in the blue ellipse

in the post-noon sector of the equatorial plane, with $\nabla_\perp \cdot \boldsymbol{J}_\perp$ where $\boldsymbol{J}_\perp$ is the FPC vector. The red circle is the projection of the area where the type L current system crosses the magnetopause to the equatorial plane as depicted in Fig. 3. Similarly, the area marked by the blue ellipse is the projection of the area where the FPC is converted to the FAC in the type H current system as depicted in Fig. 3. We recognize that some current vectors in the red circle direct inward in the magnetopause region. Thus, we need to investigate the driving mechanism of the inward current to understand why the type L current system flows across the magnetopause to understand the first issue. Next, we note that the FPC–FAC conversion for the type H current system appears in the area marked by the blue ellipse where $\nabla_\perp \cdot \boldsymbol{J}_\perp$ is negative. This region is located behind the cross-magnetopause current of the type L current system. Thus, we need to investigate the generation mechanism of negative $\nabla_\perp \cdot \boldsymbol{J}_\perp$ to understand the second issue.

Now we consider the driving mechanism of the cross-magnetopause current of the type L current system and the generation mechanism of the negative $\nabla_\perp \cdot \boldsymbol{J}_\perp$ of the type H current system. Paper 1 demonstrated that the inertia current ($\boldsymbol{J}_i = \widehat{e} \times \left(\rho \frac{\mathrm{D}\boldsymbol{v}}{\mathrm{D}t} \right)_\perp /B$) is dominant over the diamagnetic current ($\boldsymbol{J}_d = \widehat{\widehat{e}} \times \nabla_\perp p/B$) in the PI phase, where $\boldsymbol{v}$, p, and $\widehat{e}$ denote the flow vector, plasma pressure, and unit vector along the magnetic field ($\boldsymbol{B}/B$), respectively. Consequently, we examined the behavior of the inertia current in the PI phase. (In addition, it is difficult for the diamagnetic current to derive the FPC from the magnetosheath to the magnetosphere because the inward-flowing diamagnetic current in the post-noon sector needs the pressure increase toward the night-side magnetosheath.) Figure 7 shows the equatorial distribution of the inertia current at $t = 5.5$ min in the post-noon sector. Because in the red circle region, the inertia current has a component that crosses the magnetopause, we understand that the cross-magnetopause current is driven by an inertial force. Next, we recognize that the inertia current in the region between the red circle and the blue ellipse returns toward the noon direction. Furthermore, the inertia current converges in the blue ellipse. Consequently, the convergence of the FPC in the blue ellipse shown in Fig. 6 is derived from the behavior of the return inertia current. Therefore, by this return flow, the FPC–FAC conversion region for the type H current system appears behind the region where the type L current system is across the magnetopause.

To understand the behavior of the inertia current, that is, the inward cross-magnetopause FPC and negative $\nabla_\perp \cdot \boldsymbol{J}_i$ behind the region of the cross-magnetopause current in Fig. 7, we investigated the plasma flow pattern in the post-noon sector of the equatorial plane.
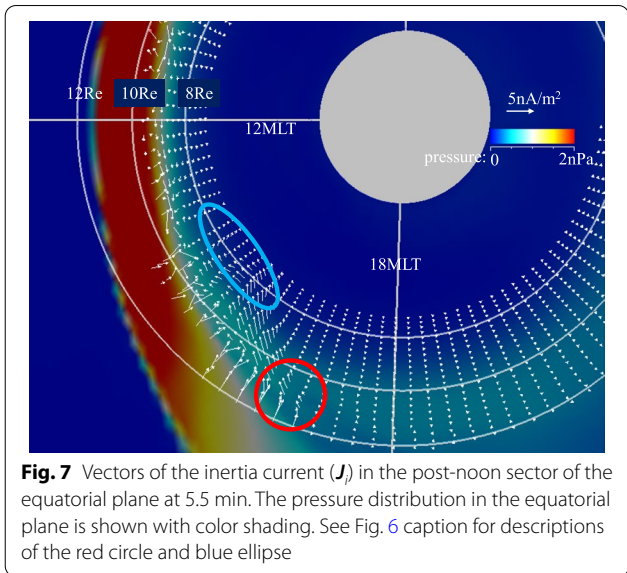

Fig. 7 Vectors of the inertia current ($\boldsymbol{J}_i$) in the post-noon sector of the equatorial plane at 5.5 min. The pressure distribution in the equatorial plane is shown with color shading. See Fig. 6 caption for descriptions of the red circle and blue ellipse
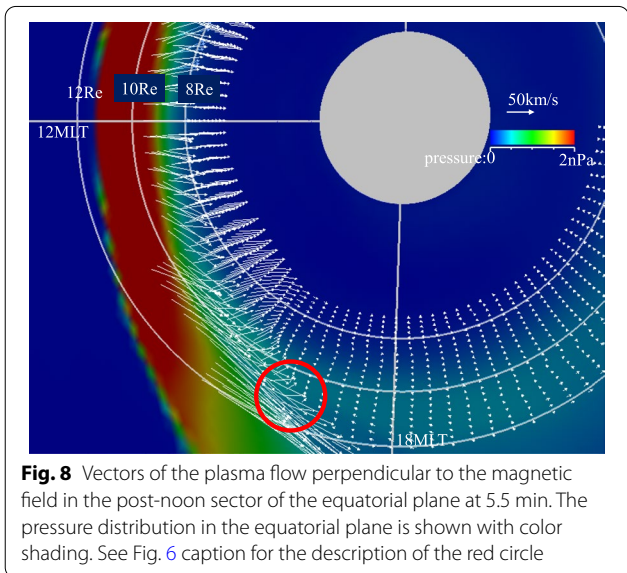

Fig. 8 Vectors of the plasma flow perpendicular to the magnetic field in the post-noon sector of the equatorial plane at 5.5 min. The pressure distribution in the equatorial plane is shown with color shading. See Fig. 6 caption for the description of the red circle

Figure 8 shows plasma flow vectors in the outer magnetosphere and the magnetosheath in the post-noon sector of the equatorial plane at $t = 5.5$ min. The color shading indicates the pressure distribution in the equatorial plane. This figure shows that the high-speed magnetosheath flow associated with the sudden compression of the dayside magnetosheath splits to the post-noon sector in the magnetosheath. This high-speed flow in the magnetosheath is caused by squeezing the plasmas in the noon magnetosheath, which is compressed by a sudden increase in the solar wind dynamic pressure. As explained below, plasmas in the front of the high-speed flow are accelerated in the anti-sunward direction along

the magnetosheath. Consequently, the inertia force in the anti-sunward direction appears in the front region of the high-speed flow in the red circle, and the inertia current driven by this acceleration generates the cross-magnetopause current from the magnetosheath to the magnetosphere. Furthermore, the flow vectors in Fig. 8 explain why the inertia current returning to the sunward direction appears behind the red circle (Fig. 7). That is to say, the flow direction gradually deflects from the anti-sunward direction to the Earthward direction in the region between the red circle and the blue ellipse. This flow pattern yields the return flow of the inertia current in the region between the red circle and the blue ellipse shown in Fig. 6.

Let us consider the reason why the high-latitude edge of the type H current system in the ionosphere does not move much in the longitudinal direction from 5.5 to 5.9 min. To explain this feature, we show in Fig. 9 the FPC vectors and $\nabla_{\perp} \cdot \boldsymbol{J}_{\perp}$ on the sphere of $r = 8$Re at $t = 5.9$ min. The FPC vectors in the region of negative $\nabla_{\perp} \cdot \boldsymbol{J}_{\perp}$ head in the sunward direction. This behavior indicates that a return inertia current appears even in the higher latitudes, as in the equatorial region shown in Fig. 6. Thus, even at higher latitudes, a negative $\nabla_{\perp} \cdot \boldsymbol{J}_{\perp}$ appears in the outer magnetosphere behind the front of the high-speed magnetosheath flow. Furthermore, the nearly concentric distribution of negative $\nabla_{\perp} \cdot \boldsymbol{J}_{\perp}$ on the sphere indicates that the deformation of the dayside magnetosheath by the SC spreads concentrically from the subsolar point. Because the dawn-dusk flow of this current at 5.9 min appears at high latitudes as shown in Fig. 4, the region where the FPC is converted to FAC shifts rather to the higher latitudes without significant

Fig. 9 FPC vectors in the post-noon sector on the sphere of $r = 8$Re in the northern hemisphere at 5.9 min. $\nabla_{\perp} \cdot \boldsymbol{J}_{\perp}$ on this sphere is shown with color shading. The red circle indicates the region through which the type L current system from B_H passes (Fig. 4)

movement toward the anti-sunward direction. Indeed, the conversion region is found in the higher latitude region, as noted with a red circle in this figure. Consequently, the ionospheric footpoint of the type H current system in the higher latitude does not move much in the longitudinal direction. Finally, we can understand the deformation of the FAC distribution in the ionosphere from the high-speed moving type L current system in the lower latitude and the nearly immovable type H current system at higher latitudes. Finally, the fact that the ionospheric footpoint of the type H current system advances from A_H at 5.5 min to B_C at 5.9 min can be explained by the concentric spread of negative $\nabla_{\perp} \cdot \boldsymbol{J}_{\perp}$.

Here, to clarify the acceleration mechanism that drives the cross-magnetopause inertia current, we explain the generation mechanism of the high-speed flow in the red circle shown in Fig. 8 from the viewpoint of energy conversion. That is to say, we show how plasmas in the red circle are accelerated. Figure 10 illustrates the equatorial distributions of (a) the work done by the inertia force $\left[\boldsymbol{v}_{\perp} \cdot \left(\rho \frac{\mathrm{D}\boldsymbol{v}}{\mathrm{D}t} \right)_{\perp} \right]$; (b) the negative work done by the pressure gradient force ($\boldsymbol{v}_{\perp} \cdot \nabla_{\perp} p$), and (c) the work done by the Lorentz force ($\boldsymbol{J}_{\perp} \cdot \boldsymbol{E}_{\perp}$). It is evident from this figure that the plasmas are accelerated in the post-noon sector of the magnetosheath $\left[\boldsymbol{v}_{\perp} \cdot \left(\rho \frac{\mathrm{D}\boldsymbol{v}}{\mathrm{D}t} \right)_{\perp} > 0 \right]$. This region corresponds to the front of the high-speed flow from Fig. 8. In addition, because $\boldsymbol{v}_{\perp} \cdot \nabla_{\perp} p < 0$ in this region, plasmas are accelerated by the pressure gradient force. When the pressure in the dayside magnetosheath increases suddenly at the onset of the SC, a steep pressure gradient appears in the post-noon sector (and pre-noon sector) of the magnetosheath. Therefore, the compressed dayside magnetosheath squeezes the plasmas in the dayside magnetosheath to the post-noon sector and pre-noon sector of the magnetosheath. Note that $\boldsymbol{J}_{\perp} \cdot \boldsymbol{E}_{\perp}$ is positive in the front region of the high-speed flow. In other words, the Lorentz force also accelerates the plasma.

Finally, we note that $\boldsymbol{J}_{\perp} \cdot \boldsymbol{E}_{\perp}$ is negative in the dayside magnetosheath and dayside magnetopause region. The dynamo of the type H current system is located in the magnetopause region. This dynamo is the same as that for the PI current system reported by Paper 1. In addition, the dynamo in the dayside magnetosheath drives the type L current system.

Discussion

Longitudinal propagation of the SC signal in the magnetosphere

Araki ([1994](#)) suggested that the front of the SC signal propagates at the speed of the fast magnetosonic wave in the magnetosphere. Moreover, it was already reported
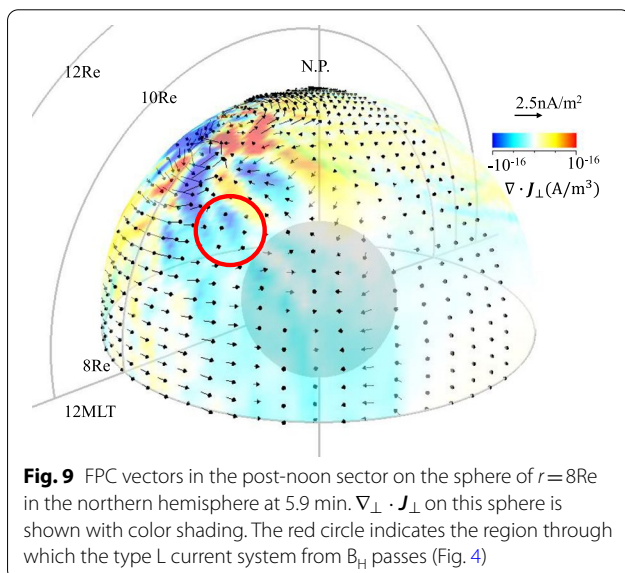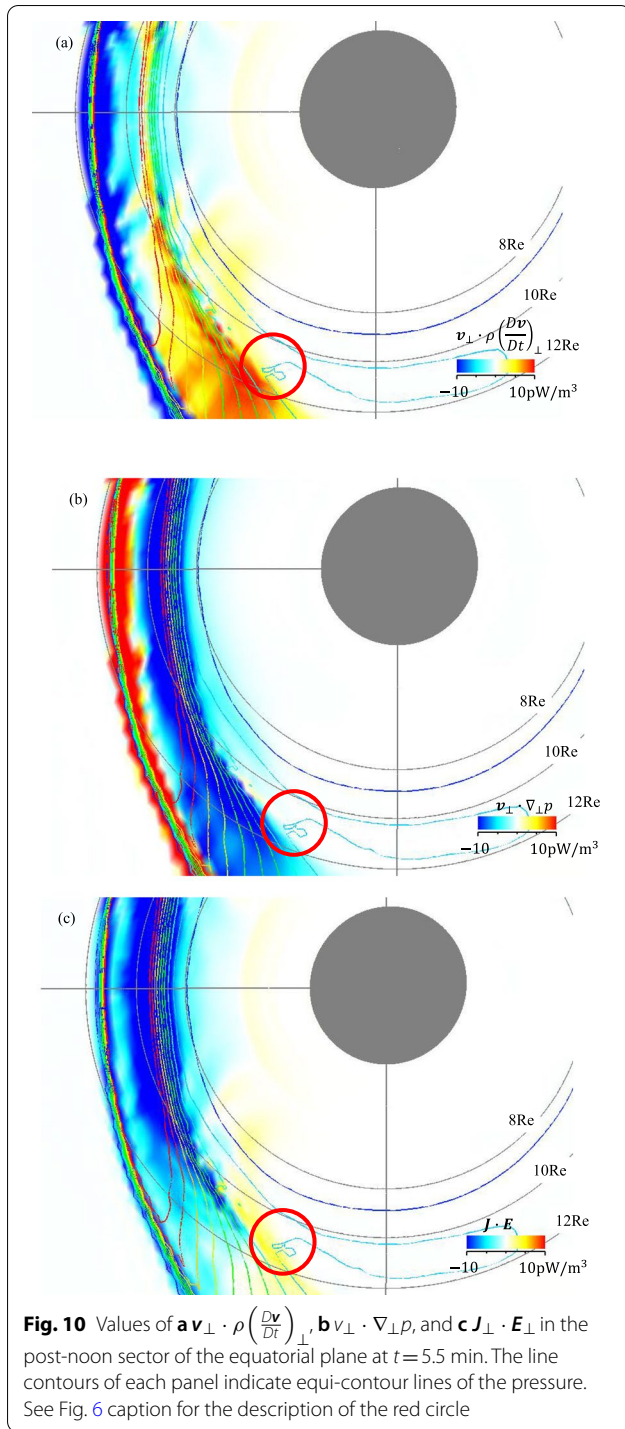
Fig. 10 Values of **a** $v_\perp \cdot \rho \left(\frac{D\mathbf{v}}{Dt} \right)_\perp$, **b** $v_\perp \cdot \nabla_\perp p$, and **c** $J_\perp \cdot E_\perp$ in the post-noon sector of the equatorial plane at $t = 5.5$ min. The line contours of each panel indicate equi-contour lines of the pressure. See Fig. 6 caption for the description of the red circle

that the magnetospheric signal propagates at the speed of the fast magnetosonic wave in the magnetosphere (e.g., Takahashi et al. 2015, 2017). However, the type L current system propagates in the anti-sunward direction at the speed of the plasma flow in the magnetosheath. This speed is slower than the fast magnetosonic wave speed.

Thus, we evaluated the relationship between the speed of the longitudinal propagation of the two current systems introduced in this paper and the magnetosonic speed of the fast magnetosonic wave.

Figure 11 depicts the temporal propagation of the plasma disturbances $\left(\left| dv/dt \right| \right)$ in the equatorial plane of the magnetosphere–magnetosheath region excited by sudden compression of the dayside magnetosphere. The SC front observed by satellites (Takahashi et al. 2015, 2017) is recognized by the propagating edge of finite $\left| dv/dt \right|$ in this figure. From Fig. 11, it is evident that the SC signal front indicated by black thick arrows appears at $t = 4.0$ min in the magnetosphere and propagates toward the nighttime magnetosphere till it arrives at the midnight magnetosphere at $t = 5.9$ min. The propagation speed is about 1000 km/s, which is comparable to the speed of the fast magnetosonic wave (the Alfvén speed) in the magnetosphere. In contrast, the SC signal speed in the magnetosheath (indicated by blue arrows) is almost the solar wind speed (372 km/s). The cross-magnetopause current of the type L current system flows in the SC signal front in the magnetosheath. Consequently, the longitudinal propagation speed of the ionospheric FAC associated with the type L current system is the solar wind speed projected onto the ionosphere. That is to say, the longitudinal propagation speed of the PI signal of the SC caused by the type L current system is slower than that of the SC front determined by the onset of the SC signal in the magnetosphere. The observational fact that the PI signal in the ionosphere propagates at the speed corresponding to the solar wind speed (Engebretson et al. 1999) can be explained by the propagation property of the type L current system. The type H current system follows behind the type L current system.

Wave modes of the PI current system

As shown in Figs. 3 and 4, the FACs in the ionosphere are converted from the FPC in the magnetosphere. The conversion was a key issue of the generation mechanism of the PI geomagnetic variations in terms of coupling of the fast magnetosonic wave and the Alfvén wave (Tamao 1964). It is noted that this conversion occurs in the dayside magnetosphere where the plasma β is low. The low β plasma contains the Alfvén wave and the fast magnetosonic wave. Thus, before investigating the FPC–FAC conversion, it is instructive to examine whether the PI current has the nature of the Alfvén-mode current or that of the fast magnetosonic-mode current. In this section, we describe the investigation of the wave modes of the currents both for the type L current system and for the type H current system. In addition, we consider the relationship between the PI current system found by
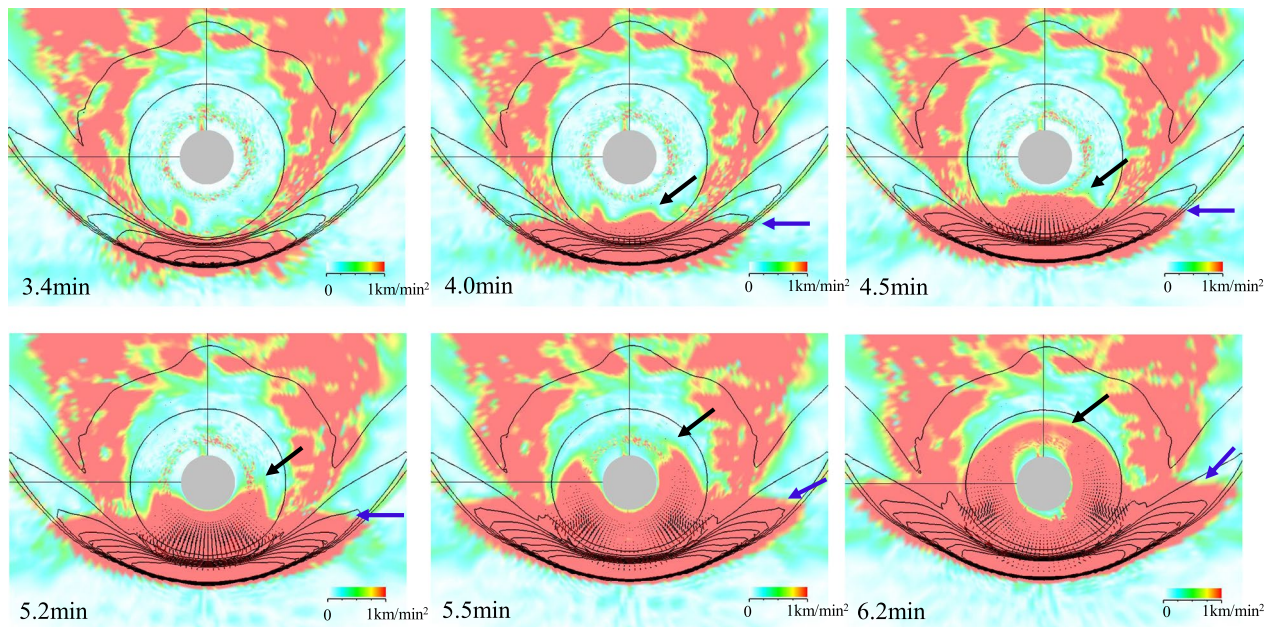
Fig. 11 Temporal spread of the magnetospheric SC signal front, indicated as the edge of the positive region of $|\frac{dv}{dt}|$. The black and blue arrows in the panels of $t=4.0$ min to $t=6.2$ min indicate the SC front in the magnetosphere and the magnetosheath, respectively. It is evident that the SC front arrives at the night-side magnetosphere at 6.2 min, when the PI current system in the ionosphere does not reach the nightside. The line contours show the pressure in the equatorial plane. Irregular patterns of $|\frac{dv}{dt}|$ in the night-side magnetosphere are fluctuations. We do not discuss the fluctuations in this paper because they do not play any roles in the propagation of the SC signal

Paper 1 and the type H and type L current systems shown in this paper.

We evaluated the relative importance of the two MHD waves on the current lines shown in Fig. 3. Because the Alfvén wave and the fast magnetosonic wave are characterized by the divergence of the electric field ($\nabla_\perp \cdot \boldsymbol{E}_\perp$) and the field-aligned component of the electric field vortex [$\widehat{e} \cdot (\nabla \times \boldsymbol{E}_\perp)$], Fig. 12 presents the current lines of the type L current system and the type H current system with the line color of $\epsilon = \frac{\nabla_\perp \cdot \boldsymbol{E}_\perp}{|\nabla_\perp \cdot \boldsymbol{E}_\perp| + |\widehat{e} \cdot (\nabla \times \boldsymbol{E}_\perp)|}$ at $t=5.5$ min. Only the part of the current line in the area with plasma $\beta < 0.2$ is shown in this figure. When ϵ is close to 0 or ± 1, the current belongs to the fast magnetosonic wave or the Alfvén wave, respectively. From this figure, we recognize that both the type H current system and the type L current system in the inner magnetosphere denoted by (1) have the nature of the Alfvén wave. Next, the dawn-to-dusk current of the type H current system in the outer magnetosphere has the nature of the fast magnetosonic wave. In addition, the cross-magnetopause current of the type L current system has the same nature, too. Both current lines are denoted by (2). Third, we need to discuss the mode of the current connecting the dawn-to-dusk FPC and the FAC of the type H current system along the current lines of (3). We already observed that the dawn-to-dusk FPC of the type H current system
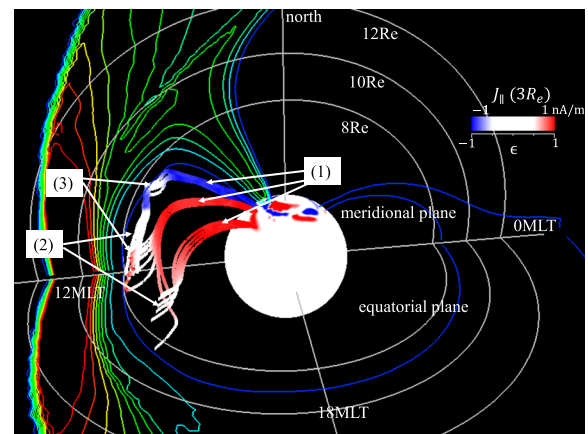

Fig. 12 The type H and L current systems illustrated in the same manner used in Fig. 3 at $t=5.5$ min according to the value of ϵ. The current lines are shown only in the area of $\beta<0.2$. The Alfvén-mode current and the fast magnetosonic-mode current are dominant along the current lines denoted by (1) and (2), respectively. The mixture of the two modes appears along the current lines denoted by (3)

seems to be directly converted to the FAC in Fig. 3 because the white current (FPC) curve seems to connect to the red (FAC) one. In contrast, the mode of the current connecting the FPC and the FAC is instead the fast

magnetosonic wave from Fig. 12 because the color of the current line is white in this figure. This simulation result indicates that the current in the region (3) is a mixture of the Alfvén wave and the fast magnetosonic wave. These patterns are discussed in the next section from the viewpoint of the FPC–FAC conversion.

In the last part of this section, let us discuss the PI current system found by Paper 1. Figure 3 shows that the type H current system from A_H at $t=5.5$ min, located in the boundary between two regimes, possesses the short FPC between the dawn-to-dusk current and the FAC. This short FPC flows toward the magnetosphere. (The type H current system from B_C at $t=5.9$ min also consists of the upward/downward FACs and the FPC along the magnetopause, as well as the short FPC that turns toward the Earth from Fig. 4). Figure 12 also indicates that this short current flowing to the magnetosphere has the nature of the fast magnetosonic wave. While the PI current system found by Paper 1 has the FPC between the FAC connecting to the ionosphere and the dawn-to-dusk current along the magnetopause. In addition, Paper 1 discussed that the FPC belongs to the fast magnetosonic wave. Therefore, the type H current system near the transition between the type L current system regime and the type H current system regime is the same as the PI current system found in Paper 1. Thus, the PI current system found by Paper 1 is categorized as the type H current system that appears in the area between the type H current system regime and the type L current system regime.

Conversion mechanism between the FAC and the FPC

FAC generation in the PI phase has been investigated in the context of conversion from the fast magnetosonic wave to the Alfvén wave (e.g., Tamao 1964; Fujita et al. 2003a). However, we note that the Alfvén wave has both the FAC and FPC because the displacement current associated with the Alfvén wave flows perpendicular to the magnetic field. Consequently, the mode conversion theory does not completely explain how the FPC is converted to the FAC in Fig. 3. In addition, the previous studies treated the mode conversion only qualitatively. Besides, we have the grid-point values of the FPC and the FAC that satisfy the physical principles of the MHD equations. Therefore, we can discuss rigorously the conversion between the FPC and the FAC. That is to say, we use the conservation of the electric current in the magnetic flux as follows:

$$\nabla_\parallel \left(\frac{J_\parallel}{B}\right) + \frac{\nabla_\perp \cdot \boldsymbol{J}_\perp}{B} = 0, \tag{1}$$

where $J_\parallel$ is the FAC. We also use the wave mode information shown in Fig. 12 to interpret the FPC–FAC conversion. Here we investigated the mechanism of the

FPC–FAC conversion shown in Fig. 3. (We discuss only Fig. 3 here because the conversion shown in Fig. 4 is essentially the same as that in Fig. 3.)

First, because the inertia current is dominant in the PI phase, we examined $\nabla_\perp \cdot \boldsymbol{J}_i/BJ$ instead of $\nabla_\perp \cdot \boldsymbol{J}_\perp/BJ$ in the type H current system and the type L current system at $t=5.5$ min, as shown in Fig. 13. (Hereafter, we ignore the type L current system from A_H.) When $\nabla_\perp \cdot \boldsymbol{J}_i < 0$, the FPC is converted to the FAC. This FAC generation is located in the region where the FPC from the cross-magnetopause current becomes the FAC for the type L current system at the boundary between the inner and outer magnetospheres, and in the region where the dawn-to-dusk current turns to the FAC in the post-noon sector in the outer magnetosphere for the type H current system. These regions are denoted by (1). Meanwhile, the FPC generation ($\nabla_\perp \cdot \boldsymbol{J}_i > 0$) appears in the region where the FAC turns to the dawn-to-dusk current in the pre-noon outer magnetosphere for the type H current system. This region is denoted by (2). These results are consistent with the FPC–FAC conversion shown in Fig. 3. Finally, $\nabla_\perp \cdot \boldsymbol{J}_i > 0$ is also evident in the lower part of the inner magnetosphere in the post-noon sector for both current systems, and $\nabla_\perp \cdot \boldsymbol{J}_i < 0$ appears in the upper part of the inner magnetosphere in the pre-noon sector in the type H current system. These regions are denoted by (3). [$\nabla_\perp \cdot \boldsymbol{J}_i$ in the region (3) will be discussed in "Inertia 3" section] It is noted here that the FAC is not generated in the high-β and low-β transition region (Tanaka 2007) because the
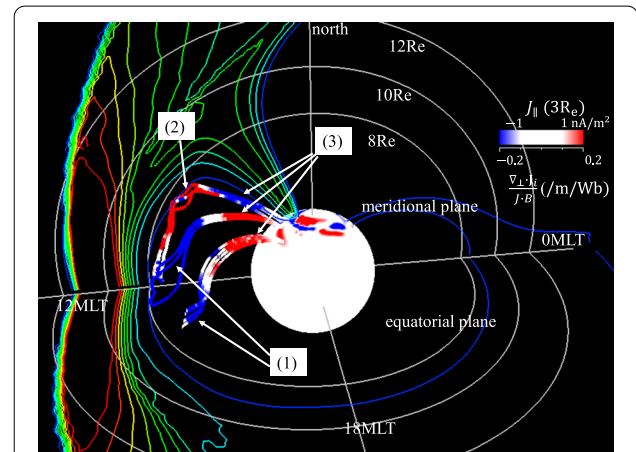

Fig. 13 Type H and L current systems at $t=5.5$ min colored according to $\frac{\nabla_\perp \cdot \boldsymbol{J}_i}{JB}$ values in the same manner as in Fig. 3. The current lines are shown only in the area of $\beta<0.2$. The type L current from A_H is not shown in this figure. There are three characteristic regions of the FPC–FAC conversion. The negative and positive $\frac{\nabla_\perp \cdot \boldsymbol{J}_i}{JB}$ in regions (1) and (2), respectively, appears in the boundary between the outer and inner magnetospheres. The region (3) is located in the lower magnetosphere

diamagnetic current in the PI phase is not effective in the dayside magnetosphere.

To investigate the mechanism of $\nabla_\perp \cdot \boldsymbol{J}_i$ presented in Fig. 13, we divide $\nabla_\perp \cdot \boldsymbol{J}_i/BJ$ into the following five terms:

Inertia 1:

$$+\rho\left(\frac{\mathrm{D}\boldsymbol{v}}{\mathrm{D}t}\right)_\perp \cdot \frac{2\widehat{e}\times\nabla_\perp\mathrm{B}}{B^3J}, \tag{2}$$

Inertia 2:

$$-\rho\left(\frac{\mathrm{D}\boldsymbol{v}}{\mathrm{D}t}\right)_\perp \cdot \frac{\widehat{e}\times\nabla_\perp\rho}{\rho B^2J}, \tag{3}$$

Inertia 3:

$$-\frac{\rho\widehat{e}}{B^2J} \cdot \nabla \times \left(\frac{\mathrm{D}\boldsymbol{v}}{\mathrm{D}t}\right)_\perp, \tag{4}$$

Inertia 4:

$$+\rho\left(\frac{\mathrm{D}\boldsymbol{v}}{\mathrm{D}t}\right)_\perp \cdot \frac{\widehat{\phi}}{R_cB^2J}, \tag{5}$$

Inertia 5:

$$+\rho\left(\frac{\mathrm{D}\boldsymbol{v}}{\mathrm{D}t}\right)_\perp \cdot \frac{\nabla\times\boldsymbol{B}}{B^3J}, \tag{6}$$

where R_c is the radius of curvature of the magnetic field line, $\widehat{\phi}$ is the unit vector azimuthal to the magnetic field line defined as $\widehat{e} \times \widehat{n}$, and $\widehat{n}$ is the unit vector normal to the magnetic field $[\widehat{n} = -(\widehat{e} \cdot \nabla)\widehat{e}/R_c]$. Details of the inertia terms are discussed below.

Inertia 1 and inertia 2

Inertia 1 and inertia 2 are the FPC–FAC conversion due to the spatial gradient of the magnetic field intensity and the conversion due to the spatial gradient of plasma density, respectively. [Note that inertia 1 corresponds to Eq. 4 of Vasyliunas (1970) by changing the inertia force to the pressure gradient force.] After some algebraic operations, Eqs. (2) and (3) become

$$\rho\left(\frac{\mathrm{D}\boldsymbol{v}}{\mathrm{D}t}\right)_\perp \cdot \frac{2\widehat{e}\times\nabla B}{B^3J} - \rho\left(\frac{\mathrm{D}\boldsymbol{v}}{\mathrm{D}t}\right)_\perp \cdot \frac{\widehat{e}\times\nabla\rho}{\rho B^2J} = \left(\frac{\mathrm{D}\boldsymbol{v}}{\mathrm{D}t}\right)_\perp \cdot \frac{\widehat{e}\times\nabla V_A^2}{\mu_0 V_A^4}, \tag{7}$$

where V_A is the Alfvén speed. Therefore, it is sufficient to examine the right-hand term of Eq. (7) to investigate the effect of the spatially changing plasmas in the magnetosphere during the FPC–FAC conversion. We call this term inertia V_A (Positive and negative patterns of both inertia 1 and inertia 2 show the same distribution along the current as that of inertia V_A). Figure 14 shows the type H current system and the type L current system colored according to inertia V_A. When we compare the distribution of the relative importance of the Alfvén wave in the two MHD waves (ϵ in Fig. 12) in the current
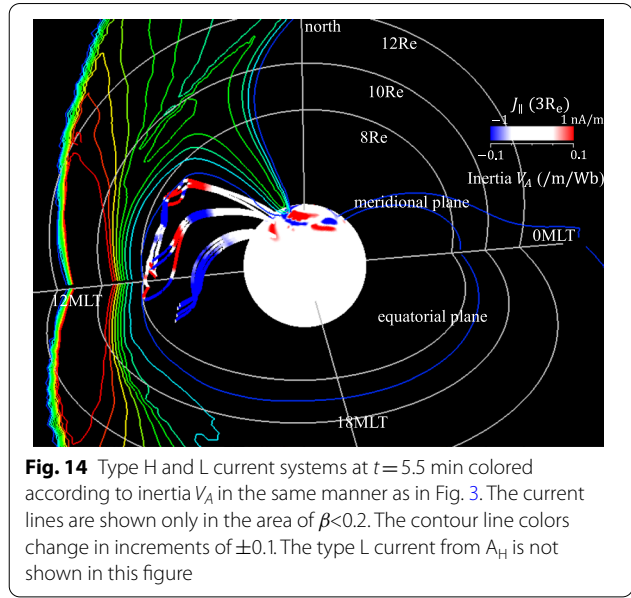

Fig. 14 Type H and L current systems at $t = 5.5$ min colored according to inertia V_A in the same manner as in Fig. 3. The current lines are shown only in the area of $\beta < 0.2$. The contour line colors change in increments of ± 0.1. The type L current from A$_H$ is not shown in this figure

systems with that of inertia V_A, we recognize that inertia V_A has non-zero values in the region where the fast magnetosonic wave has at least a non-zero contribution (the color of the current line is pale red → yellow → white). Therefore, Figs. 12 and 14 confirm that inertia V_A refers to mode conversion from the fast magnetosonic wave to the Alfvén wave due to the spatial gradient of V_A.

Next, we investigated the implication of the inertia V_A change on the type L current system shown in Fig. 14. Inertia V_A exhibits negative behavior in the upper part of the inner magnetosphere and adjacent outer magnetosphere. This result indicates that the FPC of the fast magnetosonic wave is converted to the FAC of the Alfvén wave. In other words, the Alfvén wave of the type L current system is recharged by the fast magnetosonic wave due to the spatial gradient of V_A in the upper part of the inner magnetosphere and adjacent outer magnetosphere. We first tried to understand this mode conversion by analyzing the plasma behavior shown in Fig. 8. Figure 15 illustrates the distribution of V_A in the equatorial plane and in the 14.4 MLT meridian (the local time of the type L current), as well as the type L current system with the line color of V_A. From Fig. 8, $\boldsymbol{v}_\perp$ is directed toward the Earth with a slight tilt to the anti-sunward direction in the region $L > 7$. Thus, the ϕ component of $\boldsymbol{v}_\perp$ is positive. Because $\left(\frac{\mathrm{D}\boldsymbol{v}}{\mathrm{D}t}\right)_\perp$ is almost parallel to $\boldsymbol{v}_\perp$, $\left(\frac{\mathrm{D}\boldsymbol{v}}{\mathrm{D}t}\right)_\perp$ has a positive ϕ component. Next, the term, $\widehat{e} \times \nabla V_A$ in Eq. (7) was estimated as $\widehat{e} \times \left(-\widehat{n} \cdot \left|(\widehat{n} \cdot \nabla)V_A\right|\right) = -\widehat{\phi}\left|(\widehat{n} \cdot \nabla)V_A\right|$. From Fig. 15, V_A in the outer magnetosphere exhibits a smaller but non-zero spatial gradient toward the Earth. Therefore,
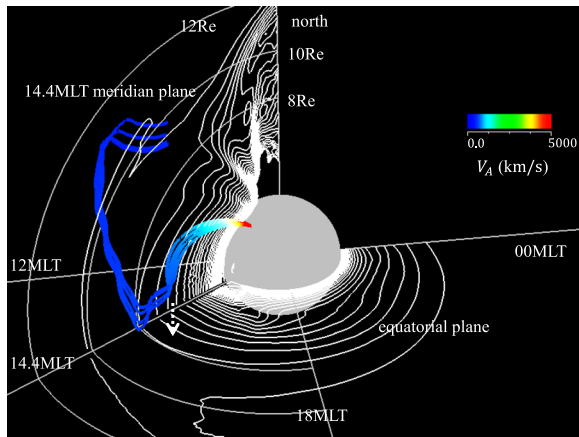
Fig. 15 Distributions of V_A in the 14.4 MLT meridian plane and the equatorial plane. The type L current system that flows in the 14.4 MLT plane is also shown. The white dotted arrow indicates the L value of the field line where FPC is converted to FAC ($L \approx 7$). The color of the current lines denotes V_A

Fig. 16 Type H and L current systems at $t = 5.5$ min colored according to inertia 3 values in the same manner as in Fig. 3. The current lines are shown only in the area of $\beta < 0.2$. The contour line colors change in increments of ± 0.2. The type L current from A_H is not shown in this figure. The inset in the left-bottom corner shows an enlarged part of the footpoints of both current systems. The color scale of inertia 3 for the inset is in increments of ± 0.05

$|(\hat{n} \cdot \nabla) V_A|$ is positive. Consequently, $\left(\frac{D\boldsymbol{v}}{Dt}\right)_\perp \cdot (\hat{e} \times \nabla V_A)$ becomes negative. Thus, we can understand that inertia V_A becomes negative in the outer magnetosphere. [In physical terms, the sudden compression of the dayside magnetosphere induces the fast magnetosonic wave ($\boldsymbol{v}_\perp$ in Fig. 8), which is converted to the Alfvén wave due to the spatial gradient of V_A]. As a result, the FPC of the type L current system turns into the FAC in the region where V_A starts to increase toward the inner magnetosphere. Meanwhile, Fig. 12 indicates that the Alfvén wave is predominant in the inner magnetosphere and that the fast magnetosonic wave does not arrive there. Therefore, inertia V_A becomes almost zero in the inner magnetosphere because there is no fast magnetosonic wave, although the spatial gradient of V_A is enhanced in the inner magnetosphere. In other words, this area is not the region where the spatial gradient of V_A is steep, for example, the plasmapause region, as suggested by Paper 1. This mechanism determines the lower latitude boundary of the FAC of the PI in the ionosphere.

The behavior of inertia V_A on the type H current system is rather complicated compared with that of the type L current system. It shows roughly two negative regions and one positive region in the post-noon magnetosphere. That is, the FAC is recharged from the fast magnetosonic wave in the near-equatorial region of the outer magnetosphere, it then charges the fast magnetosonic wave in the neighboring region between the inner and outer magnetospheres, and it again recharges the fast magnetosonic wave in the upper edge part of the inner magnetosphere. This structure is related to the
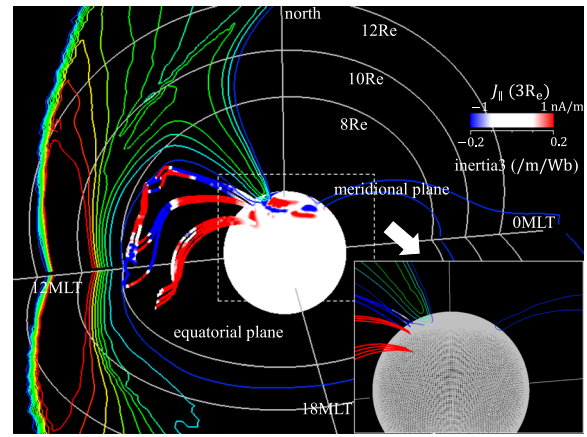
profile of inertia 3 in the type H current system. Thus, this feature of inertia V_A in the type H current system is discussed below.

Inertia 3
Inertia 3, shown in Fig. 16, is related to the Alfvén wave because $\hat{e} \cdot \nabla \times \left(\frac{D\boldsymbol{v}}{Dt}\right)_\perp$ is roughly proportional to $\nabla_\perp \cdot \boldsymbol{E}_\perp$. Therefore, this term represents the conversion between the displacement current (FPC) and the FAC within the Alfvén wave. To show the behavior of inertia 3 in the lower boundary, the inset in the left-bottom corner shows an enlarged part of the footpoints of both current systems. The color scale of inertia 3 for the inlet is given in increments of ± 0.05.

First, we describe the characteristic features of inertia 3 in the type L current system. It is essentially positive from the lower boundary to the outer magnetosphere in the post-noon sector. This feature indicates that the Alfvén wave is recharged by the fast magnetosonic wave due to the spatial gradient of V_A in the upper part of the inner magnetosphere and the outer magnetosphere (Fig. 14). On the way to the ionosphere, the displacement current of the Alfvén wave diverges from the field line. It is noted that inertia 3 has smaller values but is still positive in the lower boundary region, as seen in the inset of Fig. 16. The positive inertia 3 near the lower boundary can be understood as demonstrating that the electric current in the ionosphere has positive divergence because the PI current in this region flows into the ionosphere. The smaller inertia 3 near the lower boundary implies that the PI electric field

induced in the ionosphere may be suppressed by the conducting ionosphere.

Second, inertia 3 in the type H current system in the post-noon sector is positive in the lower half part of the inner magnetosphere, and the sign reverses in the upper half. It is noted that inertia V_A in the inner magnetosphere in Fig. 14 is negative in the region where inertia 3 is zero. At the same time, $\nabla_\perp \cdot \boldsymbol{J}_i$ is also negative (Fig. 13) in the upper part. These results allow us to conclude that convergence of the inertia current (Fig. 6) yields an increase in the FAC of the Alfvén wave (negative inertia 3 in Fig. 16) and an increase in the FPC of the fast magnetosonic wave (positive inertia V_A in Fig. 14). It is noted that the inertia 3 of the Alfvén wave exhibits a field-aligned structure with a node in the inner magnetosphere. In the outer magnetosphere, the Alfvén wave and the fast magnetosonic wave are mixed in the current lines between the dawn-to-dusk current and the FAC of the type H current system. Therefore, inertia 3 and inertia V_A have different signs alternately.

Finally, we discuss whether the behavior of inertia 3 indicates excitation of a standing Alfvén wave. First, the type L current system has smaller inertia 3 in the lower boundary (the ionosphere) and is positive on the current lines. The plasma disturbances in the dayside magnetosphere are symmetric with respect to the equatorial plane, and inertia 3 is positive in the southern hemisphere. Therefore, the global field-aligned profile of inertia 3 exhibits a wave of the field line with nodes in the northern and southern ionospheres and an antinode at the equator. Consequently, the fundamental standing Alfvén wave may be generated in the lower latitude part of the PI current system. However, the wave structure of the field line of the FAC part of the type H current system has positive inertia 3 in the lower part of the inner magnetosphere in both hemispheres and a negative one in the equatorial region. Thus, nodes will appear in between the lower boundary (the ionosphere) and the equator. Therefore, the Alfvén wave with the third harmonic structure is possibly excited in the higher-latitude part of the PI current system. The global MHD simulation cannot reproduce the standing Alfvén wave because of its numerical diffusion. Thus, the simulation does not reproduce the standing waves noted above. To confirm this possible standing wave is a future issue.

Inertia 4
Inertia 4 represents the FPC–FAC conversion due to curvature of the magnetic field line. When the magnetic field is almost a dipole field, we obtain

$$\frac{\widehat{e} \times \nabla B}{B^3} \simeq \frac{\nabla \times \widehat{e}}{B^2} = \frac{\widehat{\phi}(\widehat{n} \cdot \nabla) B}{B^3} \simeq -\frac{\widehat{\phi}}{R_c B^2}. \tag{8}$$

Therefore, the curvature effect (inertia 4) is half the size of inertia 1, and the sign is reversed. As a result, this term does not play an important role in the conversion between the FPC and FAC.

Inertia 5
Inertia 5 is derived by modification of the magnetic field direction caused by the current. Eventually, this term can be deformed like

$$\rho\left(\frac{\mathrm{D}\boldsymbol{v}}{\mathrm{D}t}\right)_\perp \cdot \frac{\nabla \times \boldsymbol{B}}{B^3 J} = \rho\left(\frac{\mathrm{D}\boldsymbol{v}}{\mathrm{D}t}\right)_\perp \cdot \frac{\boldsymbol{J}_\perp}{\mu_0 B^3 J} = \rho\left(\frac{\mathrm{D}\boldsymbol{v}}{\mathrm{D}t}\right)_\perp \cdot \frac{\boldsymbol{J}_d}{\mu_0 B^3 J}, \tag{9}$$

where μ_0 is the magnetic permeability of a vacuum. This term is not effective in the magnetosphere compared with other terms because $\boldsymbol{J}_d$ is not significant in the dayside magnetosphere.

Ionospheric latitudes of the PI current system
To conclude our discussion, we will focus on the ionospheric latitude of the PI current system. This latitude corresponds to the magnetic field line where the FPC is converted to the FAC. The ionospheric latitude of the PI current in the higher latitudes (the type H current system) is related to the area where the return inertia current exhibits convergence near the post-noon magnetopause as shown in Fig. 6. (The current shows divergence near the pre-noon magnetopause although this is not shown in this figure). This is located at $L \approx 8$. While the PI current in the lower latitudes (the type L current system) exhibits the conversion in the area considerably distant from the magnetopause. From Fig. 15, the FPC from the cross-magnetopause current turns to the FAC in the region where V_A begins to increase toward the Earth. This is located at $L \approx 7$. It is noted that the turning position does not exist in the region with a steep V_A gradient, although the FPC–FAC conversion occurs due to the spatial gradient of V_A. To confirm this simulation result, we need a statistical study of the FAC position of the PI. This will be future work.

Summary and conclusion
The preliminary impulse of the sudden commencement is simply explained by the generation of the compressional wave due to sudden compression of the dayside magnetopause and mode conversion from the compressional wave to the Alfvén wave in the magnetosphere. However, this simple model cannot explain a time delay of the peak displacement and longer duration time in the higher latitudes in the pre-noon and post-noon sectors of the polar region. We performed simulations of the PI current systems in the magnetosphere–ionosphere system to reveal the machenaism that there are two different current systems in the PI phase in the higher-latitude region and the lower-latitude region of the ionospheric FAC region of

the PI. The main results of this paper are summarized as follows:

1. The PI current system with the FAC in the lower-latitude ionosphere (type L current system) consists of the FAC in the inner magnetosphere and the ionosphere, the cross-magnetopause current, and the magnetosheath current. The cross-magnetopause current is the inertia current invoked by the inertia force to the anti-sunward direction in the front region of the high-speed flow invoked by compression of the dayside magnetosheath. The longitudinal propagation speed of this current system is the solar wind speed in the magnetosheath in the anti-sunward direction projected into the ionosphere. But it is considerably slower than the fast magnetosonic wave in the magnetosphere.

2. The PI current system with the FAC in the higher-latitude ionosphere (type H current system) consists of upward/downward FACs in the pre-noon/post-noon sections, respectively, and dawn-to-dusk along the magnetopause in the outer magnetosphere. This current system appears behind the type L current system. The PI current system found by Fujita et al. (2003a) is categorized as the type H current system that appears in the area between the type H current system regime and the type L current system regime.

3. The type L current system in the ionosphere propagates in the anti-sunward direction at the solar wind speed in the magnetosheath projected into the ionosphere. In contrast, the type H current system in the ionosphere appears behind the type L current system, and this current system in the sunward edge in the ionosphere almost stays in the same longitude. Therefore, the PI current distribution of the ionosphere forms a crescent shape in which the low-latitude edges extend in the anti-sunward direction and the high-latitude edges are almost stationary. Consequently, the duration of the PI ground magnetic signal becomes longer at higher latitudes, and the peak of the PI geomagnetic variations is delayed at higher latitudes.

4. The spatial gradient of plasmas induces conversion from FPC to FAC of the type L current system due to the mode conversion from the fast magnetosonic wave to the Alfvén wave. This conversion occurs in the outer magnetosphere, where the compression of the dayside magnetosphere drives the inward plasma flow that belongs to the fast magnetosonic wave. Consequently, the FPC turns into the FAC in the region where the Alfvén speed begins to increase toward the inner magnetosphere. This region does not correspond to the region with a steep spatial gradient of the Alfvén speed, like the plasmapause. This mechanism determines the low-latitude limit of the FAC of the PI in the ionosphere.

5. The FPC to FAC conversion for the type H current system occurs in the outer magnetosphere near the magnetopause. The return inertia current from the region where the type L current system crosses the magnetopause invokes negative/positive divergence in the post-noon/pre-noon sector, respectively. Thus, the type H current system always appears behind the type L current system.

6. The conversion between the displacement current (FPC) and the FAC of the Alfvén wave is dominant in the near-Earth inner magnetosphere. The divergence of the displacement current is positive in the post-noon inner magnetosphere for both the type L and type H current systems because downward FAC in the ionosphere invokes a positive divergence of the current in the ionosphere. The positive divergence of the displacement current extends along the current line of the type L current system to the outer magnetosphere. In contrast, the type H current system has a negative divergence in the outer magnetosphere because the inertia current in the post-noon sector of the outer magnetosphere exhibits convergence.

7. The fundamental standing Alfvén wave in the lower latitude side of the PI signal and the third harmonic standing Alfvén wave in its higher latitude side are possibly excited associated with the SC.

Author contributions
SF conducted the numerical simulation and analyzed the simulation results. SF and TT wrote the paper. Both the authors read and approved the final manuscript.

Author details
[1]Joint Support-Center for Data Science Research, Research Organization of Information and Systems (ROIS), Tachikawa, Tokyo 190-8518, Japan. [2]The Institute of Statistical Mathematics, ROIS, Tachikawa, Tokyo 190-8518, Japan. [3]International Center for Space Weather Science and Education, Kyushu University, Fukuoka 819-0395, Japan.

References
Araki T (1994) A physical model of the geomagnetic sudden commencement. In: Engebretson MJ, Takahashi K, Scholer M (eds) Solar wind sources of magnetospheric ultra-low-frequency waves. American Geophysical Union, Washington, D.C., pp 183–200
Belakhovsky VB, Pilipenko VA, Sakharov YA, Lorentzen DL, Samsonov SN (2017) Geomagnetic and ionospheric response to the interplanetary shock on January 24, 2012. Earth Planets Space 69:105. https://doi.org/10.1186/s40623-017-0696-1
Chapman S, Ferraro VCA (1940) The theory of the first phase of a geomagnetic storm. Terr Magn Atmos Electr 45(3):245–268. https://doi.org/10.1029/TE045i003p00245
Engebretson MJ, Murr DL, Hughes WJ, Lühr H, Moretto T, Posch JL, Weatherwax AT, Rosenberg TJ, Maclennan CG, Lanzerotti LJ, Marcucci F, Dennis S, Burns G, Bitterly J, Bitterly M (1999) A multipoint determination of the propagation velocity of a sudden commencement across the polar ionosphere. J Geophys Res 104(A10):22433–22451. https://doi.org/10.1029/1999JA900237
Fujita S, Tanaka T, Kikuchi T, Fujimoto K, Hosokawa K, Itonaga M (2003a) A numerical simulation of the geomagnetic sudden commencement: 1. Generation of the field-aligned current associated with the preliminary impulse. J Geophys Res 108(A12):1416. https://doi.org/10.1029/2002JA009407
Fujita S, Tanaka T, Kikuchi T, Fujimoto K, Itonaga M (2003b) A numerical simulation of the geomagnetic sudden commencement: 2. Plasma processes in the main impulse. J Geophys Res 108(A12):1417. https://doi.org/10.1029/2002JA009763
Sastri JH, Takeuchi T, Araki T, Yumoto K, Tsunomura S, Tachihara H, Luehr H, Watermann J (2001) Preliminary impulse of the geomagnetic storm sudden commencement of November 18, 1993. J Geophys Res 106(A3):3905–3918. https://doi.org/10.1029/2000JA000226
Takahashi N, Kasaba Y, Shinbori A, Nishimura Y, Kikuchi T, Ebihara Y, Nagatsuma T (2015) Response of ionospheric electric fields at mid-low latitudes during sudden commencements. J Geophys Res Space Phys 120:4849–4862. https://doi.org/10.1002/2015JA021309
Takahashi N, Kasaba Y, Nishimura Y, Shinbori A, Kikuchi T, Hori T, Ebihara Y, Nishitani N (2017) Propagation and evolution of electric fields associated with solar wind pressure pulses based on spacecraft and ground-based observations. J Geophys Res Space Phys 122:8446–8461. https://doi.org/10.1002/2017JA023990
Takeuchi T, Araki T, Luehr H, Rasmussenn O, Watermann J, Milling DK, Mann IR, Yumoto K, Shiokawa K, Nagai T (2000) Geomagnetic negative sudden impulse due to a magnetic cloud observed on May 13, 1995. J Geophys Res 105:18835–18846
Tamao T (1964) A hydromagnetic interpretation of geomagnetic SSC*. Rep Ionos Space Res 18:16–31
Tamao T (1965) Transmission and coupling resonance of hydromagnetic disturbances in the non-uniform Earth's magnetosphere. Sci Rep 17:43–72
Tanaka T (2007) Magnetosphere-ionosphere convection as a compound system. Space Sci Rev 133:1–72. https://doi.org/10.1007/s11214-007-9168-4
Tanaka T (2015) Substorm auroral dynamics reproduced by the advanced global M–I coupling simulation. In: Zhang Y, Paxton LJ (eds) Auroral dynamics and space weather, vol 215. AGU, Washington, D.C., p 177. https://doi.org/10.1002/9781118978719
Tanaka T, Ebihara Y, Watanabe M, Den M, Fujita S, Kikuchi T, Hashimoto KK, Kataoka R (2020) Reproduction of ground magnetic variations during the SC and the substorm form the global simulation and Biot-Savart's law. J Geophys Res Space Phys 125:e2019JA027172. https://doi.org/10.1029/2019JA027172
Vasyliunas VM, McCormac BM (1970) Mathematical models of magnetospheric convection and its coupling to the ionosphere, particles and fields in the magnetosphere. Springer Netherlands, Dordrecht, pp 60–71. https://doi.org/10.1007/978-94-010-3284-1_6